# EFFECT OF BUBBLE DIAMETER ON MODIFICATION OF TURBULENCE IN AN UPWARD PIPE FLOW

Akiko Fujiwara
Intelligent Modeling Laboratory,
The University of Tokyo,
Hongo, Bunkyo-ku, Tokyo 113-8656, Japan
fujiwara@fel.t.u-tokyo.ac.jp

Daiju Minato, Koichi Hishida
Department of System Design Engineering,
Keio University,
Hiyoshi, Kohoku-ku, Yokohama 223-8522, Japan
minato@mh.sd.keio.ac.jp, hishida@sd.keio.ac.jp

## ABSTRACT

The objective of the present study is to elucidate the effect of dispersed bubble size on turbulence modification in vertically upward driven bubbly pipe flow. The experiment was conducted with void fractions of 0.5 and 1.0%. Liquid phase velocity is measured by particle image velocimetry with fluorescent tracer particles (PIV/LIF). Bubbles' size and velocity are estimated from the bubbles' image observed by projecting shadow image technique. Bubbles strongly accumulate near the wall and slide up. The high concentration of bubbles in the vicinity of the wall induce reduction of fluctuation velocity intensity. The effect of bubble-induced turbulence on the global pipe flow structure was discussed with the turbulent energy production and dissipation are estimated from experimental data, and local vortical structure around the bubbles.

## INTRODUCTION

One of the most important aspects of multiphase flow is the interaction of the dispersed phase with turbulent flow. Knowledge of the bubbly flow is of significance to several engineering systems which include chemical reactors and bioreactors. In addition, there is interest in frictional drag reduction by micro bubbles injection on ship hulls in the field of marine engineering. In order to gain further knowledge of the effect of bubbles on turbulence modification, various experimental and numerical studies were conducted. In gas-liquid bubbly flows, past experiments in pipe flow indicated that turbulence augmentation and reduction depends on the void fraction and gas flow rate (Serizawa et al., 1975, Theofanous and Sullivan, 1982, Wang et al., 1987, Lance and Bataille, 1991). However, substantial disagreements among these experimental results can be seen in spite of experiments conducted under apparently similar conditions. One reason for this disagreement is the discord in the reported mean and *rms* values of the bubble diameter, resulting from a variety of conditions. Further, the mechanism of turbulent modulation by bubbles is still unexplored. Recently Lain et al. (2000, 2002) proposed the numerical model of turbulent bubbly flow using an Euler/Lagrangian approach. They coupled the $k$-$\varepsilon$ turbulence model and dispersed bubble equation motion simulated in a Lagrangian way. They applied this coupled methodology to simple pipe flow, and obtained good agreement with experimental data. As a first step in closure model development for bubbly turbulent flow, we need to perform the measurements under relatively simple and ideal conditions.

The objective of the present study is to elucidate the turbulence modification structure in terms of bubble diameter in a fully developed pipe flow. Specifically we aim to deduce the correlation between the global turbulence flow structure and the local turbulence modification induced by the presence of bubbles and as characterized by the instantaneous vorticity based on experimental results. Moreover we discuss the local vortical flow structure around the bubble by estimation of enstrophy from PIV/LIF data respectively.

## EXPERIMENTAL METHOD

### Measurement Technique

In order to measure the flow structure around the bubbles, specifically to detect the interaction between bubble's motion and the flow field, we applied the PIV/LIF system with Rhodamine-B as the fluorescent dye previously described by Tokuhiro et al. (1998). Figure 1 shows the measurement facility. The particles are excited by a Nd:$YVO_4$ laser sheet ($\lambda$=532nm), and fluorescence emission in the vicinity of the bubbles is detected through a color filter (which cuts off the reflection) attached to a CCD camera (left camera image). Two-dimensional velocity vector fields are obtained in time sequence. The experimental error associated with the present PIV system was estimated to be 4.3% at 95% confidence limits.

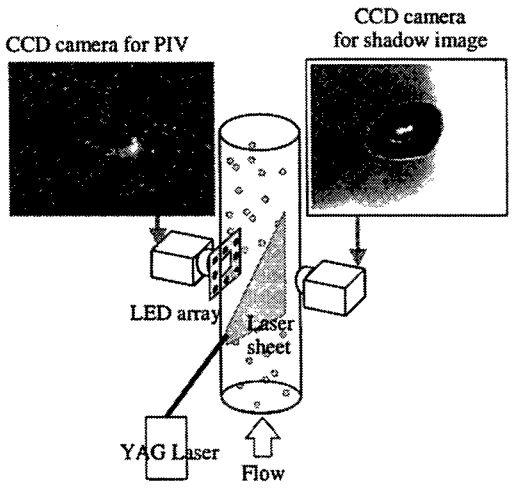


Figure 1. Schematic of Measurement Facility.

In order to capture the shape and position of bubbles simultaneously, we applied the projection technique using blue ($\lambda$=470nm) LEDs as the light source. In Figure 1 (right camera image) bubbles are illuminated from behind, and depicted in terms of a grayscale background. The focal depth of the CCD camera is approximately 6mm. Bubbles in this field have been captured at one instant of a continuous oscillatory motion. The emitted light passes through a filter attached to the CCD camera, which records the shadow image.

Our arrangement consists two CCD cameras; one for PIV/LIF (left camera in Figure 1) and the other (right camera) for detecting bubbles' shape. A square "window" within the array of LEDs provided optical access for PIV/LIF. In order to simultaneously capture both bubble shape and flow field, we synchronized the triggering of the laser, the LEDs and the two CCD cameras Figure 2 (a) and (b) shows typical snapshots took by each camera simultaneously. Velocity vector field as shown in Figure 2 (c) are reconstructed by using them.

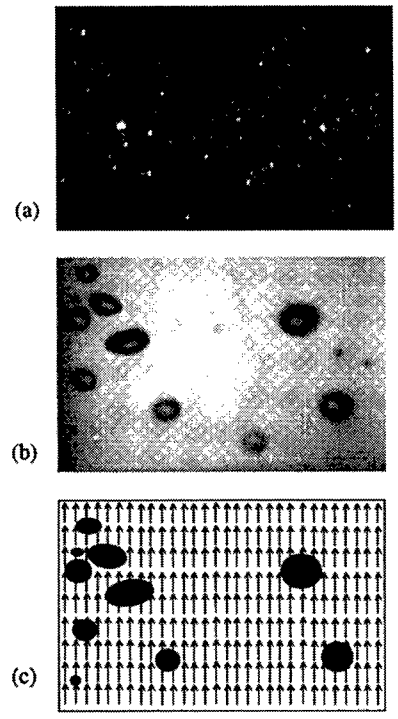


Figure 2. Typical Snapshots and Velocity Vector Field, (a) Fluorescent Tracer Particles Image, (b) Bubble Shadow Image, (c) Velocity Vector Field.

## Experimental Apparatus and Conditions

Figure 3 shows the schematic of the experimental apparatus and bubble generator. The experimental setup consists of lower and upper tanks, a vertical pipe in between them, a pump, and an air compressor. Tap water as the test fluid was flowed upward in the pipe. At the bottom of the pipe there is an entrance section with a honeycomb used to rectify the incoming flow. Up stream of the nozzle there is an air bubble generator. Figure 3 (b) shows a schematic of the bubble generator consisting of 34 of stainless steal pipe with an inner and outer diameter of 0.07mm and 0.50mm, respectively. The air pressure and flow rate was controlled by a pressure gauge and flow meter.

The test section is a 1500mm high acrylic pipe with an inner diameter, 2*R*, of 44mm. There are a few references in literature where ingenuous methods have been applied to avoid optical distortion due to refraction from the pipe. In the experiment conducted by Hosokawa et al. (2000) and Kondo et al. (2001) they used Fluorinated Ethylene Propylene copolymer (FEP) pipe in the test section. The refractive index of FEP material is approximately the same as that of water. We applied an FEP pipe in the test section.

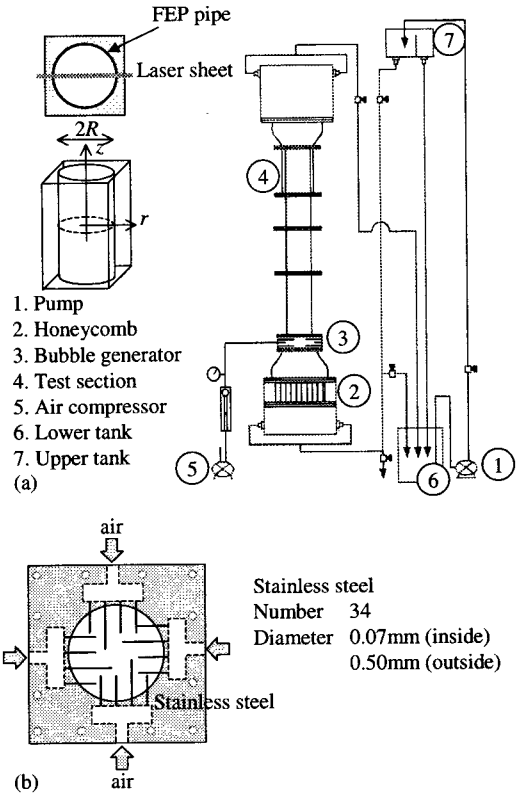


Figure 3. Schematic of Experimental Set Up, (a) Experimental Apparatus, (b) Bubble Generator.

We defined the center axis of pipe as the origin. The upward flow direction is taken to be the $z$-axis and radial direction is taken to be the $r$-axis. The laser sheet for PIV illuminated the $r$-$z$ plane.

Table 1 summarizes the experimental conditions. All the experiments were run at the bulk velocity of the single phase flow $V_{sb}$=222mm/s, corresponding to a Reynolds number of 11000 based on pipe diameter and bulk velocity. In order to compare the effect of the bubble diameter with the same void fraction, nearly 60ppm of 3-Pentanol ($C_5H_{11}OH$) was added as the surfactant. 3-Pentanol effects on bubbles to disturb coalescence each other. And there is less influence on the average void fraction. It is ensured by Figure 4 shown the probability density function (pdf) of area equivalent bubble diameter $D_{eq}$, i.e. the diameter of a circle having the same area as the bubble in two dimensions. $D_{eq}$ is estimated from the projected bubble shadow image treated by image processing techniques. In condition without surfactant, $D_{eq}$ takes the peak value at about $D_{eq}$=2.0mm. On the other hand in condition with surfactant, it takes the peak value at about 1.2mm with small dispersion. Hereafter we mentioned that the case without surfactant as $D_M$=2mm, and with surfactant as $D_M$=1mm.

Table 1. Experimental Conditions.

| | | |
|---|---|---|
| Pipe diameter | $2R$ | 44 [mm] |
| Bulk velocity (single phase) | $V_{sb}$ | 222 [mm/s] |
| Channel Reynolds number | $Re_{2R}$ | 11,000 |
| Estimated friction velocity | $v_\tau$ | 13.3 [mm/s] |
| Reynolds number | $Re_\tau$ | 320 |
| Void fraction $\alpha$ | | 0.5% ($Q_g$=220 ml/min) |
| $\alpha$ | | 1.0% ($Q_g$=450 ml/min) |
| * Refractive index of FEP | 1.338np. | |
| water | 1.333np. | |

## RESULTS AND DISCUSSIONS

### Bubbly Flow Structure in the Pipe

Figure 5 shows the mean and the fluctuation velocity profile in single-phase flow. We can identify that it was fully developed turbulent flow at the measurement area, and there is no influence of the surfactant on the turbulent structure.

We obtained instantaneous velocity vector fields in time sequence with the present measurement technique, as shown in Figure 2 (c). White spots are denoted as the bubbles. Bubbles accumulated near the wall. And in the middle pipe region, less number of bubbles existed, and the liquid phase flow was undisturbed.

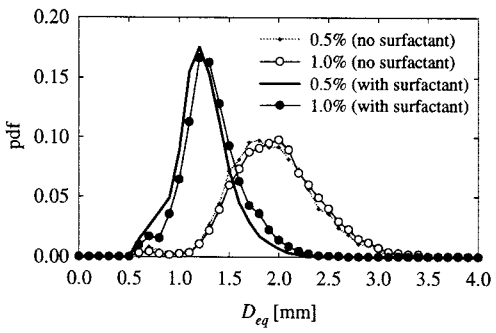


Figure 4. Effect of 3-Pentanol on pdf of Equivalent Bubble Diameter $D_{eq}$.

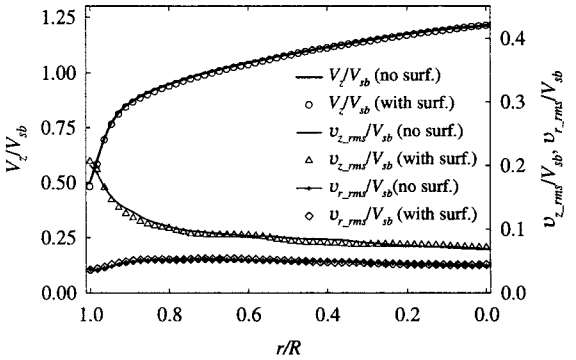


Figure 5. Effect of 3-Pentanol on Single-Phase Flow.

Average flow field is estimated from more than 1000 instantaneous velocity vector fields. Figure 6 shows the streamwise mean velocity profile for both the liquid phase and dispersed bubbles. They are normalized by the bulk velocity $V_b$ for each case. According to bubble velocity profiles, bubbles anteceded to the liquid phase in whole pipe region. Liquid phase velocity $V_z$ near the wall is faster than the single-phase velocity, and the mean stream wise velocity profile became flat (plug-like flow) for each condition. Especially for the case of small $D_M$, $V_z$ became flatter, and $V_z$ value of $\alpha$=1.0% is larger than that of 0.5% in the vicinity of the wall. In the present study at the middle pipe region, bubble velocity is more than 1.5 times larger than the liquid phase velocity. However liquid phase did not accelerate.

In Figure 7, the local void fraction $\alpha_l$ profile is estimated. Here, $\alpha_l$ is defined as the ratio of the bubble volume to the measurement volume for each $r$ position. The cross section of bubble in the perpendicular plane to $r$-$z$ plane is assumed to be a circle with the same diameter as a chord of the bubble in the $z$ direction. We projected the given diameter of the acrylic sphere that is settling in the vessel with the same technique within ±25% of accuracy.

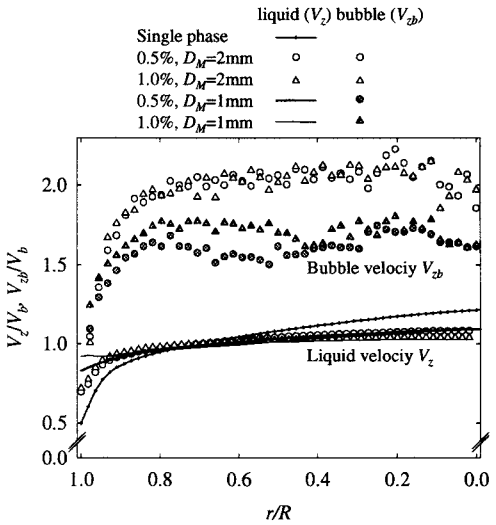


Figure 6. Streamwise Mean Velocity $V_z/V_b$ and Bubble Rising Velocity $V_{zb}/V_b$ Profiles.

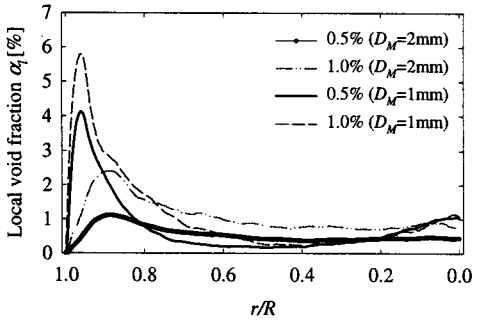

Figure 7. Local Void Fraction Profile.

According to the local void fraction profile, bubbles accumulate near the pipe wall ($r/R$>0.9), and $\alpha_l$ became high in this area for each condition. The profile of $\alpha_l$ depends on both the mean void fraction and the addition of surfactant. $\alpha_l$ takes peak value at about $r/R$=0.9 for $D_M$=2mm; on the other hand for $D_M$=1mm the peak appeared at approximately $r/R$=0.95. Accumulation of the bubbles is dominated by the lift force (Auton, 1987). It consists of the bubble mass, slip velocity of the bubble, and the vorticity around the bubble. The bubble slip velocity influenced the lift force efficiently, and small bubbles tend to move toward the wall in the present experiment. $\alpha_l$ peaks relatively closer to the wall for small $D_M$ as compared to large $D_M$ . It is noted that $\alpha_l$ peaks at nearly the same distance from the wall as $D_M$. This trend is in good agreement with the experiments conducted by Serizawa et al. (1975). Moreover the different intensity of $\alpha_l$ for the same $D_M$ condition is caused by the difference in number density of the bubbles.

Including the effects of local void fraction, bubbles ascending in the vicinity of the wall accelerated the liquid phase flow near the wall. Especially for the case with small $D_M$, most of the bubbles ascended in the region, $r/R$>0.95, thus $V_z$ in this region was faster than that in the case with large $D_M$. However the small local void fraction has less influence on average liquid phase flow structure in the middle pipe region. The mean streamwise velocity became flat in this region.

## The Effects of Bubbles on Turbulent Modification

The effects of bubbles on the turbulent structure are discussed in this section. Fluctuation velocity profiles are shown in Figure 8. In the present study the streamwise fluctuation velocity $v_{z\_rms}$ was mainly suppressed. Although $v_{z\_rms}$ has nearly same or large intensity than that in single-phase flow near the wall ($r/R$>0.9), it is suppressed rapidly in the middle pipe region, and turbulent intensity is reduced. For large $D_M$, we cannot identify the clear difference between $\alpha$=0.5 and 1.0%. However for small $D_M$, $v_{z\_rms}$ is suppressed rapidly in $\alpha$=1.0%. Considering the increase of bubble's number density in $\alpha$=1.0%, it is indicated that the reduction of turbulence occurred when the large number of bubbles ascend in the vicinity of the wall.

According to fluctuation velocity profiles in the radial direction $v_{r\_rms}$, turbulence was enhanced near the wall, and the enhanced region depends on $D_M$. This region is nearly same as the higher local void fraction region. The

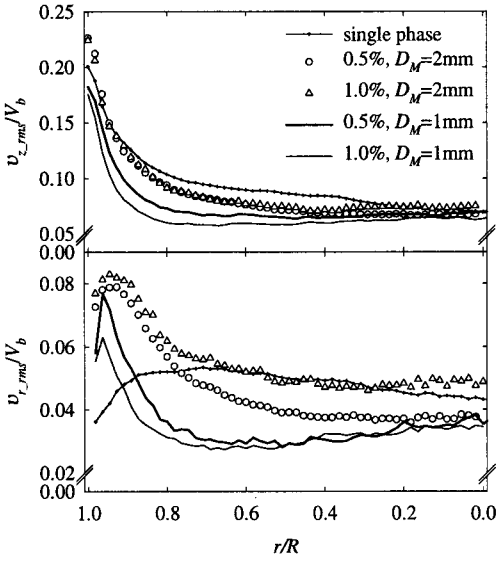

Figure 8. Fluctuation Velocity Profile of Liquid Phase in Streamwise $v_{z\_rms}$ and Radial Direction $v_{r\_rms}$.

fluctuation velocity in radial direction induced by bubbles in this region is remarkable. On the other hand in the middle pipe region, $v_{r\_rms}$ was suppressed rapidly. For small $D_M$, the same phenomenon as profile of $v_{z\_rms}$ that may be caused by the number density of bubbles occurred. However for the case of large $D_M$, $v_{r\_rms}$ is enhanced in high number density case, i.e. $\alpha$=1.0%. The wake induced by large ascending bubbles entrained the surrounding flow and perturbed it markedly. In this region the local void fraction is larger than in other cases, thus the number density of bubbles enhanced turbulence.

Figure 9 shows mean vorticity profile in $\alpha$=0.5%, and compared the effect of bubble diameter $D_M$. Vorticity, $\omega$ is estimated from circulation as described by Fujiwara et al. (2001) to avoid reduced accuracy due to differentiation of experimental data. For large $D_M$, $<\omega>$ takes nearly same or barely enhanced values as compared to single-phase flow near the wall. On the other hand for small $D_M$, the intensity of $<\omega>$ is smaller than that for single-phase flow. These results suggest that the large scale flow structure, i.e. mean velocity gradient near the wall, becomes flat due to ascending small bubbles, accordingly $<\omega>$ became flatter for this case as compared to single-phase flow. The effect of eddies induced by the wake of small bubbles did not

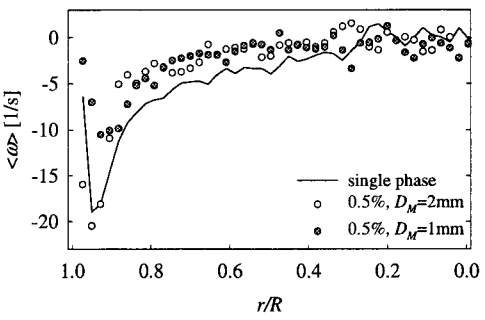

Figure 9. Mean vorticity profile of Liquid Phase in $\alpha$=0.5%.

appear in the average property.

### The Vortical Structure Around the Bubbles and Turbulent Energy Budget

In order to clarify the effect of local flow structure around the bubbles, enstrophy (instantaneous fluctuation vorticity intensity) $\Omega$ defined by

$$\Omega = (\omega - <\omega>)^2 \qquad (1)$$

is examined. The high intensity of enstrophy $\Omega$ indicates the stretching of the vortex string and changing of the vortex to small scale eddies. It means $\Omega$ has a strong correlation to turbulence energy dissipation. Figure 10 shows typical instantaneous $\Omega$ contours for two different bubble diameters at $\alpha$=0.5%. In Figure 10 high intensity of $\Omega$ appears in the region around the bubble. Especially in Figure 10 (a) the high intensity region appeared not only in the wake region but also in the inter bubble spacing. On the other hand in Figure 10 (b), bubbles accumulated in the vicinity of the wall, thus the flow accelerated by the bubbles and wall interacted resulting in the high intensity of $\Omega$. There appears a smaller uniform distribution of $\Omega$ in the middle pipe region. These results indicate significant energy dissipation occurs between the wall and bubbles. We can recognize that the region where high intensity of $\Omega$ is wide spread in the case of large $D_M$ than that in the case of small $D_M$. Since the length scale of high intensity of the vorticity is nearly the same as the bubble diameter, high intensity of $\Omega$ appeared in the region far from the wall no matter how closely the bubble ascends near the wall. Additionally the distance depends on the bubble diameter and the large bubbles ascend not only in the near wall region but also in the mid. pipe region as shown in Figure 7.

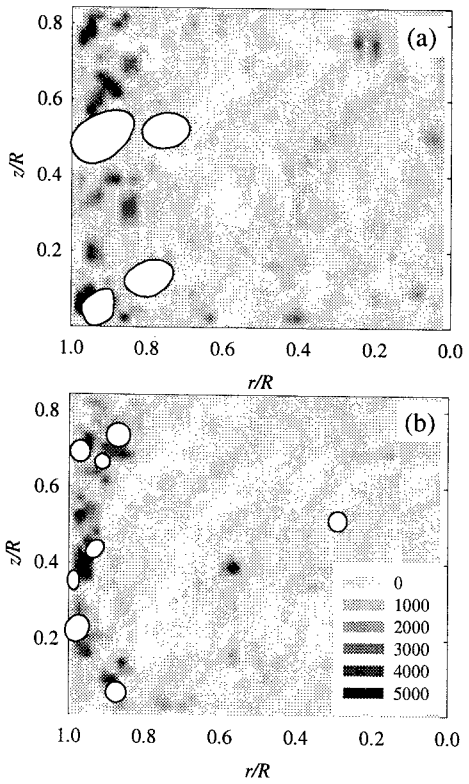


Figure 10. Instantaneous Fluctuation Vorticity Intensity $\Omega$[1/s$^2$] Contours, (a) $\alpha$=0.5%, $D_M$=2mm, (b) $\alpha$=0.5%, $D_M$=1mm.

The effect of bubbles on the turbulent energy budget will be discussed. The equation for the kinetic energy ($<v'_i v'_i>/2$) of turbulence in bubbly flow is written as

$$\frac{D\langle v'_i v'_i/2\rangle}{Dt} = P_{ij} + T_{ij} + D_{ij} + \Pi_{ij} + \varepsilon_{ij} + E_{ij} \qquad (2)$$

The terms on the right hand side of Equation 2 are: turbulent energy production, $P_{ij}$, turbulent diffusion, $T_{ij}$, viscous diffusion, $D_{ij}$, pressure gradient work, $\Pi_{ij}$ dissipation, $\varepsilon_{ij}$ and additional external force, $E_{ij}$. Although the $\Pi_{ij}$ and $E_{ij}$ terms are very important for dispersed flow, both terms are difficult to estimate experimentally. The production and dissipation terms of pipe flow are estimated by

$$P_{ij} = -\overline{v'_r v'_z}\frac{dV_z}{dr} \qquad (3)$$

$$\varepsilon_{ij} = \nu\left[\left\langle\frac{\partial v'_z}{\partial z}\right\rangle^2 + \left\langle\frac{\partial v'_r}{\partial z}\right\rangle^2 + \left\langle\frac{\partial v'_\varphi}{\partial z}\right\rangle^2 + \frac{5}{2}\left\langle\frac{\partial v'_z}{\partial r}\right\rangle^2 + \frac{5}{2}\left\langle\frac{\partial v'_z}{r\partial\varphi}\right\rangle^2\right] \qquad (4)$$

At this point, the dissipation term consists of the square of the fluctuation velocity gradient. It indicates the low accuracy. The most effective components in the dissipation term are the gradient of $v'_z$ to $r$ direction and $v'_r$ to $z$ direction. We estimated the vorticity by circulation as explained before, and the effective terms of dissipation are assumed by using fluctuation vorticity intensity, $<\omega'\omega'>$.

$$\varepsilon \cong \nu\langle\omega'\omega'_i\rangle \qquad (5)$$

Figure 11 shows turbulent energy production and dissipation profile for each condition. The production governed the average shear rate $\partial V_z/\partial r$. In addition to the flat profile of streamwise mean velocity $V_z$, Reynolds stress profile suppressed rapidly, thus the production term became small remarkably. Strictly, in the vicinity of the bubble, high intensity of average shear rate induced turbulent energy production, while there was no production in the middle pipe region.

The former experimental study conducted by Wang et al. (1987) showed the reduction of streamwise fluctuation velocity for high concentration of bubbles near the wall, and Reynolds stress became higher than single-phase flow. The difference between condition reported by Wang et al. and present study are void fraction and bubble diameter. Wang et al. conducted the experiments in more than 10% of average void fraction and large bubbles. On the other hand in the condition with small void fraction and small bubbles the two-dimensional bubbly channel flow experiment recently conducted by So et al. (2002) is in good agreement

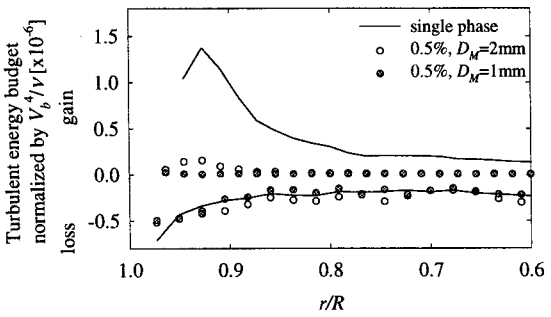


Figure 11. Turbulent Energy Budget of Liquid Phase.

with the present study. They measured the flow structure with two-dimensional laser Doppler velocimetry (LDV) and described that the high concentration of bubbles near the wall changes the flow structure to plug-like flow. The fluctuation velocity and Reynolds stress are reduced markedly in the case of high concentration of bubbles in the vicinity of the wall. They explained the remarkable suppression of Reynolds stress with stress balance considerations.

$-\nu\langle\omega'\omega'\rangle$ profile as dissipation is shown in Figure 11. While there are some assumptions to be proved Equation (5), $-\nu\langle\omega'\omega'\rangle$ is plotted to discuss the effect of bubbles on turbulent energy budget. Dissipation takes high value near the wall for each condition, and it is difficult to identify the different conditions. These results suggested that for the present conditions, bubble wake induced turbulent energy dissipation directly. Bubbles have less influence on the dissipation rate statistically because of low local void fraction.

These results suggest that the accumulation of the bubbles in the vicinity of the wall accelerated the liquid phase, and induced turbulent energy production in the vicinity of the wall, while the local flow structure around the bubbles affected the turbulent energy dissipation directly. Therefore, the turbulent energy produced near the wall could not be transferred to the middle pipe region.

## CONCLUSIONS

The investigation of vertical pipe flow injected with dispersed bubbles has been conducted using PIV/LIF, and projecting shadow image technique. For the case of high intensity of void fraction in the vicinity of the wall, average streamwise velocity profile became flat, and turbulence intensity and Reynolds stress reduced dramatically in a wide region of the pipe. The enhanced region depends on the bubble diameter, i.e., the region is nearly same as the higher local void fraction region.

From examination of turbulent energy production and enstrophy as the turbulence energy dissipation, the following mechanisms are suggested: Production term is nearly zero for mean velocity became flat and mean velocity gradient was negligibly small; on the other hand dissipation occurred around the bubble due to bubble-induced turbulence.

The fluctuation velocity induced by bubbles has slight correlation between each $z$ and $r$ component, thus the Reynolds stress is small. Further it indicates that transport of turbulent energy produced near the wall toward the middle pipe region is difficult.

## ACKNOWLEDGEMENT

This research was carried out as part of the research activity at the Center for Smart Control of Turbulence and funded by MEXT.

## REFERENCE

Auton, T. R., 1987, "The lift force on a spherical body in a rotational flow", *J. Fluid Mech.*, Vol. 183, pp. 199-218.

Fujiwara, A., Takahashi, T., Tokuhiro, A. and Hishida, K., 2001, "Turbulent microscale structure in bubbly channel flow", *4th Int. Conference on Multiphase Flow*, New Orleans, Louisiana, USA, CD-ROM

Hosokawa, S., Takesaka, K., Tomiyama, A. and Kondo, Y., 2000, "LDV measurement of Reynolds stresses in gas-liquid two-phase bubbly flow in a vertical pipe", *2nd Japan-Korea symposium on nuclear thermal hydraulics and safety, Fukuoka, Japan, October 15-18*, pp. 247-252.

Kondo, Y., Hosokawa S., Kanzawa, R. and Tomiyama, A., 2001, "Measurement of Reynokds stress of gas-liquid two-phase bubbly flow in a vertical pipe", *JSME Thermal Engineering Conference, Okayama*, pp. 393-394.

Lain,S, Bröder, D. and Sommerfeld, M., 2000, "Numerical modeling of the hydrodynamics in a bubble column using the Euler-Lagrange approach", *Proc. Int. Symp. Multiphase Flow and Transport Phenomena, Antalya (Turkey).*

Lain,S, Bröder, D., Sommerfeld, M. and Göz M.F, 2002, "Modeling hydrodynamics and turbulence in a bubble column using the Eular-Lagrange procedure," *Int. J. Multiphase Flow*, Vol 28, pp.1381-1407.

Lance, M. and Bataille, J., 1991, "Turbulence in the liquid phase of a uniform bubbly air-water flow", *J. Fluid Mech.*, Vol. 222, pp. 95-118.

Serizawa, A., Kataoka, I. and Michiyoshi, I., 1975, "Turbulence Structure of Air–Water Bubbly Flow- II. Local Properties", *Int. J. Multiphase Flow*, Vol. 2, pp. 235-246.

So, S., Morikita, H., Takagi, S and Matsumoto, Y., 2002, "Laser doppler velocimetry measurement of turbulent bubbly channel flow", *Experiments in Fluids*, Vol. 33, pp. 135-142.

Theofanous, T. G., and Sullivan, J., 1982, "Turbulence in two-phase dispersed flows", *J. Fluid Mech.*, Vol. 116, pp. 343-362.

Tokuhiro, A., Maekawa, M., Iizuka, K., Hihsida, K., and Maeda, M., 1998, "Turbulent flow past a bubble and ellipsoid using shadow-image and PIV techniques", Int. J. of Multiphase Flow, Vol. 24, pp. 1383-1406.

Wang, S. K., Lee, S. J., Jones Jr, O. C. and Lathey Jr, R. T., 1987, "3-D Turbulence Structure and Phase Distribution Measurements in Bubbly Two-Phase Flows", Int. J. Multiphase Flow, Vol. 13, No. 3, pp. 327-343.